CHEMPHYSCHEM

DOI: 10.1002/cphc.201100772

Electron Transport through Single π-Conjugated Molecules Bridging between Metal Electrodes

Manabu Kiguchi* and Satoshi Kaneko[a]

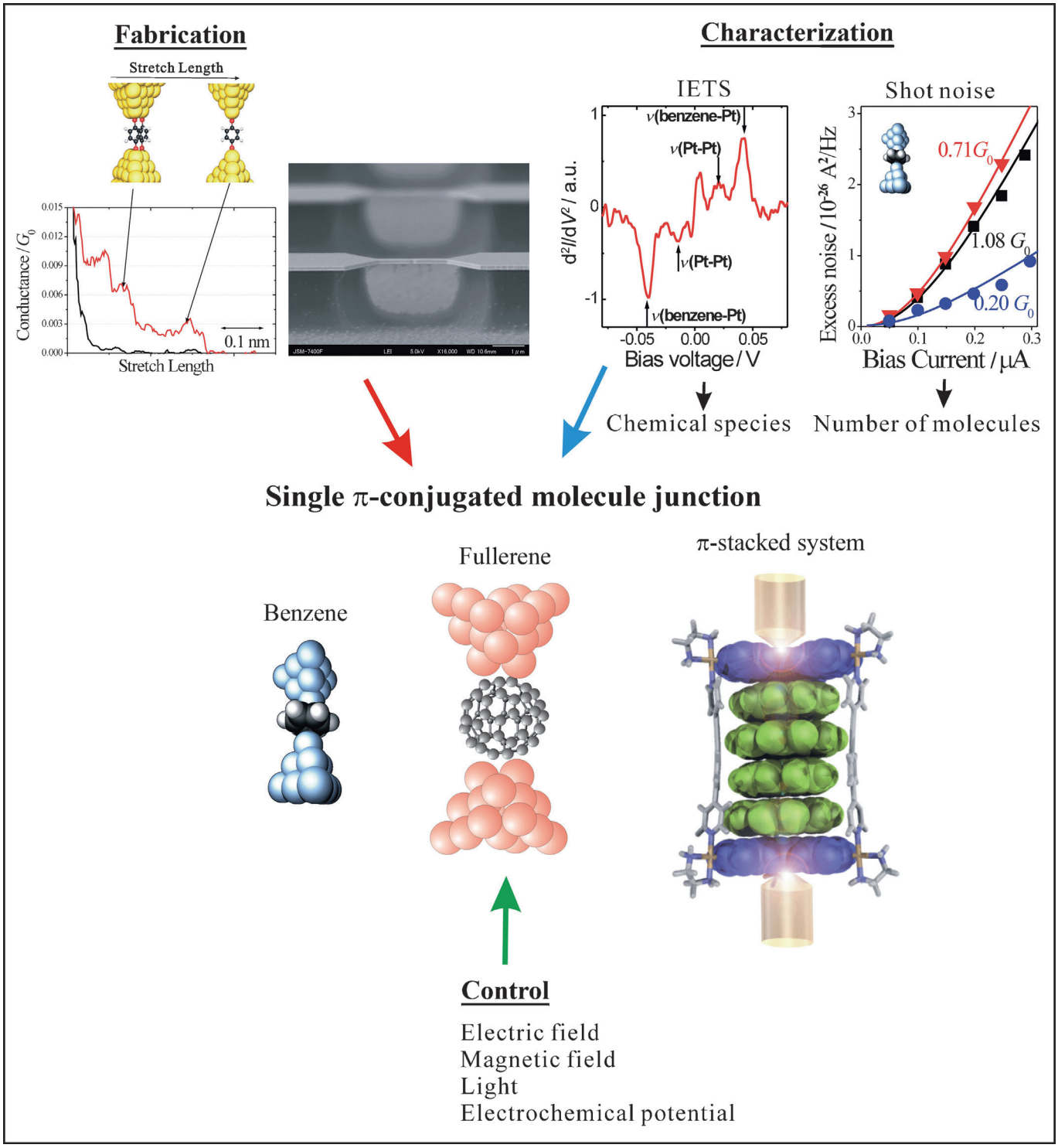

Understanding electron transport through a single molecule bridging between metal electrodes is a central issue in the field of molecular electronics. This review covers the fabrication and electron-transport properties of single π-conjugated molecule junctions, which include benzene, fullerene, and π-stacked molecules. The metal/molecule interface plays a decisive role in determining the stability and conductivity of single-molecule junctions. The effect of the metal–molecule contact on the conductance of the single π-conjugated molecule junction is reviewed. The characterization of the single benzene molecule junction is also discussed using inelastic electron tunneling spectroscopy and shot noise. Finally, electron transport through the π-stacked system using π-stacked aromatic molecules enclosed within self-assembled coordination cages is reviewed. The electron transport in the π-stacked systems is found to be efficient at the single-molecule level, thus providing insight into the design of conductive materials.

1. Introduction

Single-molecule junctions, in which a single molecule bridges the gap between metal electrodes, have attracted widespread attention due to their potential application in ultrasmall electronic devices.[1] The single-molecule junction is a low-dimensional structure that has two metal/molecule interfaces, and thus can exhibit novel physical properties that are not observed in the bulk phase. The use of a single molecule in electronic devices was first proposed by Aviram and Ratner in 1974.[2] They showed the asymmetric current–voltage characteristic for an asymmetric single molecule consisting of a donor π system and an acceptor π system, separated by a methylene tunneling bridge, by theoretical calculation. In 1997, Reed et al. succeeded in experimentally measuring the conductance of a single 1,4-benzenedithiol (BDT) molecule bridging between Au electrodes.[3] The single BDT molecule junction was fabricated using the mechanically controllable break junction (MCBJ) technique at room temperature. Tao's group reported the simple conductance measurement technique using scanning tunneling microscopy (STM) in 2003.[4]

At present, various single-molecule junctions (e.g. H_2, benzene, porphyrin, polymers, DNA) have been fabricated using MCBJ, STM, and other techniques.[5–9] To further develop the research field of the single-molecule junction, a schematic approach to these junctions (with respect to their fabrication, characterization, and control) is critically important (see Figure 1). First, fabrication of stable single-molecule junctions is required to investigate their basic properties and to use them as electronic devices. Second, the single-molecule junction should be characterized to understand its properties. Third, it is important to control the properties of the single-molecule junction by some external field, such as an electric field, light, electrochemical potential, or a magnetic field. The utilization of stable single-molecule junctions as well as their characterization is essential to understand the associated control mechanisms.

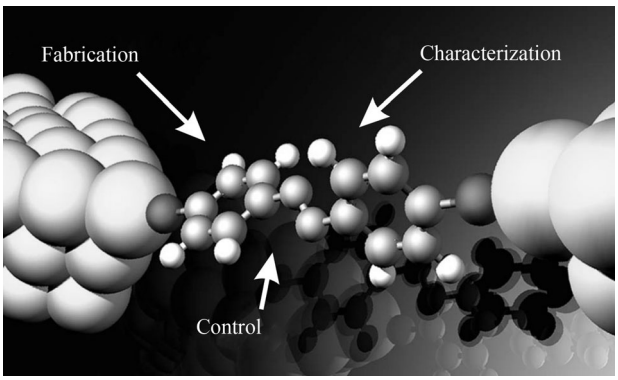

Figure 1. Single-molecule junction.

To fabricate stable single-molecule junctions, we have to pay attention to the metal/molecule interface as it plays a decisive role in determining the stability and conductance of the single-molecule junction. The current through the single-molecule junction is represented by $I(V) = \frac{2e^2}{h}\int dE T(E)[f_L(E) - f_R(E)]$, where $f_L(E)$, $f_R(E)$, and $T(E)$ are the Fermi distribution functions of the left and right electrodes, and the transmission of the single-molecule junction, respectively. In the tunneling model, $T(E)$ can be represented by $T(E) = \frac{1}{2}\sum_k \frac{(2\pi\beta^2\rho C_{rk}C_{sk}^*)^2}{(E-\varepsilon_k)^2+\eta_k^2}$, where β, ρ, C_{rk}, C_{sk} and ε_k represent the hopping integral between the metal and molecular orbitals (MOs), local density of states (LDOS) of metals at the Fermi level (E_F), the kth MO coefficient at site r and site s, and the kth MO energy, respectively. The infinitesimal η_k is determined by a Green's function and the DOS.[10] The value of β directly depends on the nature of the metal/molecule interface. Other parameters also depend on the metal/molecule interface, and its effect on the conductance of the single-molecule junction has been investigated based on this model (see Figure 2).

The single-molecule junctions have been characterized by point contact spectroscopy (PCS), inelastic electron tunneling spectroscopy (IETS), shot noise, thermoelectricity measurement, as well as other techniques. PCS and IETS have been applied to single-molecule junctions (e.g. H_2, benzene, alkanedithiol, C_{60}) to determine the chemical species bridging between metal electrodes.[5,6,11–15] The internal vibrational modes and the vibrational modes between the metal and molecule were detected by IETS and PCS. Detailed investigations have been performed of the activity of the vibration modes in the case of a single alkanedithiol molecule.[13,14] The crossover between PCS and IETS has been discussed for the highly conductive single H_2O molecule junctions. Simultaneous conductance and

[a] *Dr. M. Kiguchi, S. Kaneko*
Department of Chemistry Graduate School of Science and Engineering
Tokyo Institute of Technology
2-12-1 W4-10 Ookayama, Meguro-ku, Tokyo 152-8551 (Japan)
E-mail: kiguti@chem.titech.ac.jp

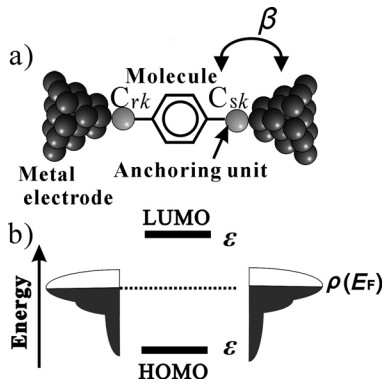

Figure 2. a) Schematic view and b) energy diagram of the single-molecule junction. β, $\rho(E_F)$, C_{rk}, and ε are the hopping integral between the metal and MOs, the local density of states (LDOS) of metals at the Fermi level (E_F), the kth MO coefficient at site r, and the MO energy, respectively.

shot noise measurements were applied to the single H_2, H_2O, and benzene molecule junctions to determine the number of conduction channels (molecules) bridging between metal electrodes.[6,16,17] The single benzene molecule junction was characterized by this simultaneous conductance and shot noise measurements. The electronic structure of the single-molecule junction was characterized by performing thermoelectric measurements. Reddy et al. measured the thermoelectric voltage for a single benzene dithiol molecule bridging between Au electrodes in solution.[18] The thermoelectric measurement revealed that electrons were transported through the HOMO and the energy difference between the Fermi level and the HOMO was 1.2 eV.

Control and functionalization of the single-molecule junction is currently a topic of great interest. Rectification behavior was observed for a single dipyrimidinyl-diphenyl molecule junction using the STM break-junction technique.[19] In this technique, the orientation of the nonsymmetric molecule was controlled through a selective deprotection strategy. Dulic et al. showed the conductance change induced by photoirradiation using photochromic molecules.[20] The resistance of the single-molecule junction after switching was about three orders of magnitude larger than that of the initial value. Song et al. succeeded in tuning the conductance of the single alkanedithiol and BDT molecule junctions by gate voltage.[21] Specifically, they used a 3-nm-thick Al_2O_3 layer as a gate dielectric. However, although these research endeavors are pioneering, it is still hard to control specific properties of the single-molecule junction. For example, molecules from the conducting to the insulating state were observed while the reverse process was not observed in the case of the single-molecule junction in which photochromic molecules were used.[20]

Currently, the single-molecule junction has become a very broad field that touches on a wide variety of topics. We cannot cover all of these topics comprehensively so, instead, we focus on the first topic: fabrication of the single-molecule junction. In particular, we pay attention to how to connect a π-conjugated molecule to metal electrodes to obtain a highly conductive single-molecule junction.

Manabu Kiguchi studied molecular vibrations on metal surfaces using X-ray absorption fine structure in Prof. Toshiaki Ohta's research group at Tokyo University, Japan, and received his Ph.D. in 2000. Beginning in 1999, as an assistant professor he studied thin films on metal surfaces in Prof. Koichi Saiki's group at Tokyo University. In 2004, he began his study of single atoms and molecular junctions in Prof. Kei Murakoshi's group as a lecturer at Hokkaido University. In 2005, he studied vibrational spectroscopy of single molecules in Prof. Jan van Ruitenbeek's group at Leiden University. Then in 2009 he was appointed associate professor of the Department of Chemistry at Tokyo Institute of Technology. His current research interests focus on nanomaterials, including single-molecule junctions and nanographene

Satoshi Kaneko is a graduate student in the Department of Chemistry at Tokyo Institute of Technology. He has studied the electrical properties of single-molecule junctions since he joined the group of A/Prof. Kiguchi in 2009.

2. Fabrication of the Single-Molecule Junction

Figure 3 shows the formation process of a single-molecule junction. By stretching the metal contact, its diameter is decreased and a single metal atomic contact is formed just before it is broken. A nanogap is formed between metal elec-

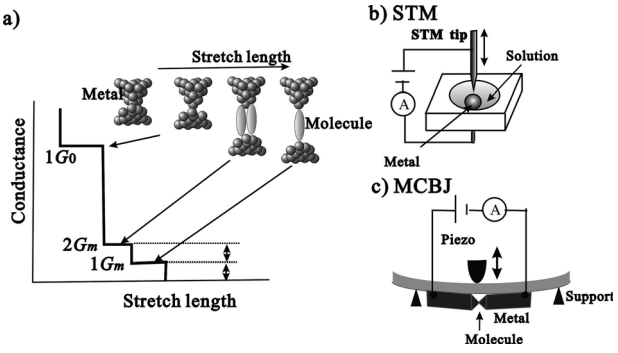

Figure 3. a) Schematic view of the formation process and conductance of the single-molecule junction during stretching of the metal contact. b) STM system to investigate the single-molecule junction fabricated in solution. c) MCBJ system to investigate the single-molecule junction.

trodes after breaking the contact and, when the metal contact is broken in the presence of molecules, the molecules can be trapped in the nanogap, thereby forming the molecular junction. The number of molecules bridging between metal electrodes decreases as the junction is stretched. Finally, a single-molecule junction is formed, just before the junction is broken.

Figure 3a shows the conductance of the contact as a function of stretching. The 1 G_0 plateau corresponds to the Au atomic contact. Just before breaking the molecular junction, conductance decreases in a stepwise fashion, with each step occurring at integer multiples of a certain value (G_m in Figure 3a), corresponding to the single-molecule conductance.

Single-molecule junctions can be fabricated using the MCBJ and STM break junction (BJ) techniques.[22] Figure 3b shows a schematic view of the STM-BJ system using Au electrodes in solution. In aqueous solution, the STM tip was coated with a wax to eliminate ionic conduction and an STM tip was repeatedly moved into and out of contact with a metal substrate in the solution containing molecules.

Figure 3c shows a schematic view of the MCBJ system. A notched metal wire was fixed to the top of a bending beam which was mounted in a three-point configuration. The metal wire was broken by mechanical bending of the substrate and cleanly fractured surfaces were exposed. The bending was then relaxed to form atomic-sized contacts between the wire ends using a piezo element for fine adjustments. The single-molecule junction could then be fabricated by breaking the metal wire in the presence of molecules using the MCBJ technique. Junctions fabricated using MCBJ are more stable than those fabricated using STM-BJ. The stability of the single-molecule junction depends on the length of the freestanding part, L, in Figure 4a. L can be decreased to submicrometer lengths using lithographic techniques. Dulic et al. succeeded in creating single-molecule junctions with lifetimes of up to 1 week.[23]

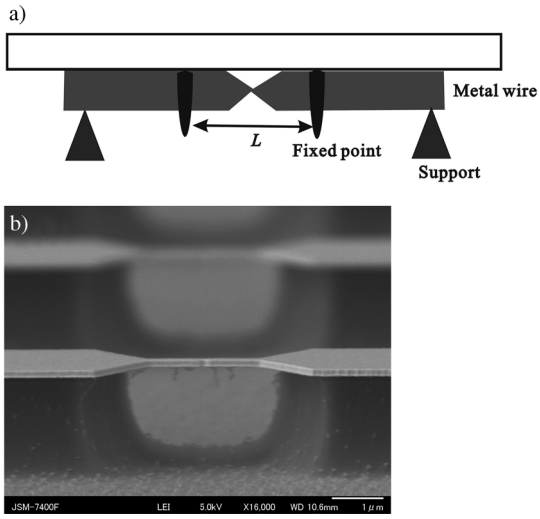

Figure 4. a) Schematic side view of the mounting of a MCBJ. b) SEM image of a lithographically fabricated MCBJ device for gold.

3. Single-Molecule Junction with Anchoring Groups

In most single-molecule junctions, molecules are bound to metal electrodes via anchoring groups such as -SH or -NH_2. By using anchoring groups, strong chemical bonds are formed between molecules and metal electrodes, which lead to the formation of stable single-molecule junctions.

The effect of the anchoring groups on the conductance of the single-molecule junctions has been investigated for disubstituted alkane molecules terminated with -SH, -NH_2, or -COOH.[24] The conductance decreased in the order -SH > -NH_2 > -COOH and the dependence of the molecule–metal contact on the conductance of the single disubstituted alkane molecule junction was explained by the strength of the molecule–metal bond, which was related to β. The relative bond strength is Au–S > Au–NH_2 > Au–COOH bond. The order of the bond strength is in accordance with the order of the conductance of the single-molecule junctions. The metal electrode dependence has been investigated for single 1,4-disubstituted (-NC and -SH) benzene molecule junctions.[25,26] The conductance of the 1,4-disubstituted benzene molecules bridging between Pt electrodes were one order larger than those bridging between Au electrodes. The higher conductance values of the single-molecule junctions with Pt electrodes were explained by the high LDOS (ρ) of Pt metal at the Fermi level.

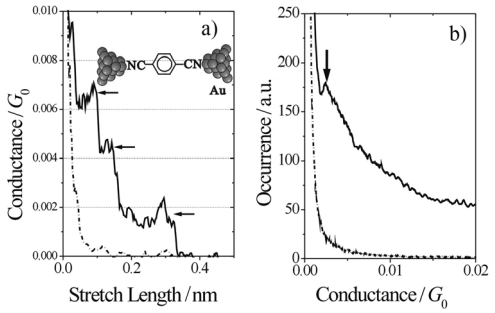

Figure 5. a) Typical conductance trace and b) conductance histogram of Au contacts broken in a tetraglyme solution containing 1,4-diisocyanobenzene. The dot-dashed line shows the result in the absence of molecules.[25]

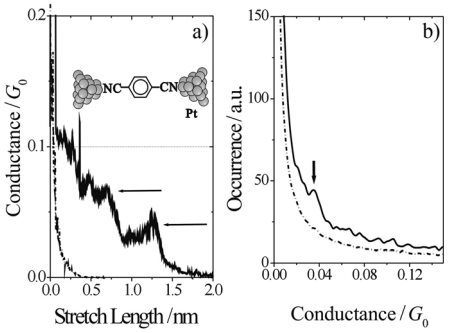

Figure 6. a) Typical conductance trace and (b) conductance histogram of Pt contacts broken in a tetraglyme solution containing 1,4-diisocyanobenzene. The dot-dashed line shows the result in the absence of molecules.[26]

Figures 5 and 6 show the conductance traces and histograms of the Au and Pt contacts in a tetraglyme solution containing 1,4-diisocyanobenzene. The conductance decreased in a stepwise fashion with each step occurring at an integer multiple of $\approx 3\times10^{-3}\ G_0$ ($3\times10^{-2}\ G_0$) for the Au (Pt) contacts. The corresponding conductance histogram showed a peak at $3\times10^{-3}\ G_0$ ($3\times10^{-2}\ G_0$; see Figures 5b and 6b). The steps in the conductance trace and a peak in the conductance histogram originate from the single 1,4-diisocyanobenzene molecule junction. The conductance values of the single 1,4-diisocyanobenzene/Au and 1,4-diisocyanobenzene/Pt junctions were determined to be $(3\pm1)\times10^{-3}$ and $(3\pm1)\times10^{-2}\ G_0$, respectively, by repeated conductance measurements (more than 3000 times). Figure 7a shows a summary of the single disubstituted benzene molecule junctions together with their conductance values.

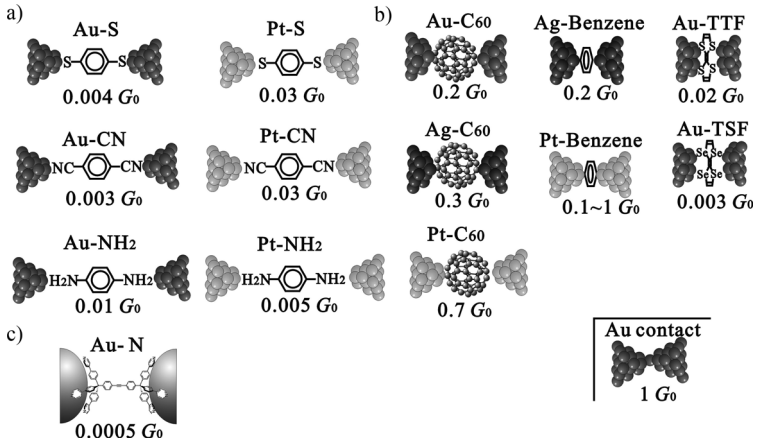

Figure 7. View of the single-molecule junctions together with their conductance values. a) Single-molecule junctions with anchoring groups, b) single-molecule junctions without anchoring groups, c) single-molecule junction with multiple anchoring units. TTF = tetrathiafulvalene, TSF = tetraselenafulvalene.

In conventional single-molecule junctions, a molecule binds to both metal electrodes via a single bond. High stability and conductivity can be expected for the single-molecule junction, in which a molecule binds to the metal electrodes via multiple bonds. Ie et al. reported the single-molecule junction with tripodal anchoring units (see Figure 7c)[27] and successfully synthesized a series of tripodal pyridine-containing molecules. The tripodal structure had a great advantage with respect to absorption efficiency compared to a single pyridine contact. The conductance of the single-molecule junction with the tripodal anchoring units was $5\times10^{-4}\ G_0$, which was substantially higher than that of previously reported shorter π-conjugated chains with single-pyridine anchors.[28] Theoretical calculations have shown that the π* orbital of the pyridine part directly interacted with the electrodes, thus leading to high conductivity of the single-molecule junction with tripodal anchoring units.

Single-molecule junctions often show various conductance values depending on the atomic configuration of the metal/molecule interface.[24,29–31] In the case of the alkanedithiol, the single-molecule junction showed two or three different conductance values which were explained by a difference between adsorption sites (atop, bridge, hollow). Venkataraman et al. tried to develop a new anchoring group to obtain single-molecule junctions showing fixed conductance values.[32–34] They showed that the spread in conductance values was much smaller for the single-molecule junction with an Au–NH_2 bond than those with Au–S, Au–CN, or Au–COOH bonds. The bonding between Au and NH_2 is a simple delocalization of the lone pair of electrons from the amine nitrogen to Au atoms. The Au–NH_2 bond is thus not strongly directional and relatively insensitive to the local structure, which leads to the small spread in the conductance values. Theoretical calculation results gave another reason for the small spread in the conductance values. The strength of the Au–NH_2 bond is weak compared to that of the conventional anchoring group (e.g. Au–S, Au–CN).[35] Only one adsorption geometry is energetically possible for the single-molecule junction with the Au–NH_2 bond, whereas different adsorption geometries with very distinct transport properties are almost equally probable for other anchoring groups. Venkataraman and co-workers showed that dimethyl phosphines (PMe_2) and methyl sulfides (SMe) are also promising anchoring groups that can be used to obtain single-molecule junctions with well-defined conductance.[36]

4. Direct Binding of π-Conjugated Molecules to Metal Electrodes

While stable single-molecule junctions can be fabricated using anchoring groups, the metal-anchoring group contact acts as a resistive spacer between the electrodes and the molecule, thus leading to low conductivity. To improve the device operation of single-molecule electronic devices, the fabrication of single-molecule junctions showing high and fixed conductance values is important. Recently, highly conductive single-molecule junctions have been fabricated by direct binding of π-conjugated organic molecules to metallic electrodes without the use of anchoring groups. The delocalized π molecular orbital directly hybridizes with the metal orbital. Figure 7b gives a summary of single-molecule junctions without anchoring groups together with their conductance values.

4.1. Benzene/Pt Junction

Benzene is a simple model system of π-conjugated molecules. A single benzene molecule junction was fabricated using the MCBJ technique in ultrahigh vacuum (UHV) at 4 K.[6] Benzene was introduced to the Pt contact using a leak valve via a heated capillary. The benzene molecular junction was characterized with IETS and simultaneous conductance and shot noise measurements.

Figure 8c shows the differential conductance (dI/dV) of the benzene/Pt junction as a function of voltage. A symmetric upward step in the differential conductance was observed around 40 mV, and peaks were observed in its derivative ($d^2I/$

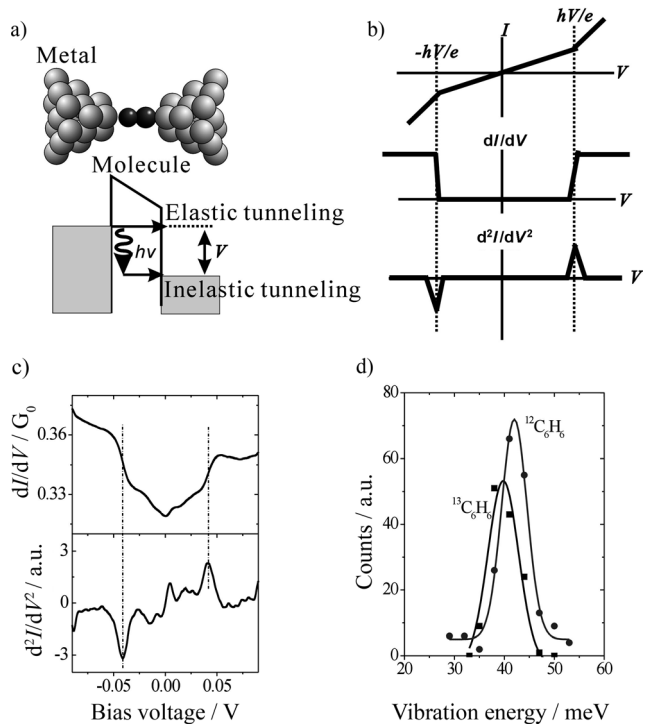

Figure 8. a) Illustration of the inelastic electron tunneling process in the single-molecule junction. b) Expected *IV*, d*I*/d*V*, and d^2*I*/d*V*^{2} curves. c) Differential conductance (top) and its derivative (bottom) for a Pt contact after the introduction of benzene taken at a zero-bias conductance of 0.3 G_0. d) Distribution of vibrational energies of the benzene/Pt junction.[6]

dV^2: IETS). The upward step in d*I*/d*V* indicates the excitation of vibrational modes by conduction electrons with energies of 40 meV (see Figure 8 a,b).[11–15] To accurately determine the vibrational energy, 250 differential conductance spectra were collected for the benzene/Pt junctions with a zero bias conductance of 0.05–0.4 G_0. Figure 8 d shows the distribution of these vibrational energies. The histogram shows a well-defined peak at 42 meV with a width of 5 meV. The IETS spectra were measured for the isotope-substituted benzene $^{13}C_6H_6$. The histogram obtained from 130 differential conductance spectra for $^{13}C_6H_6$/Pt junctions shows a peak at 40 meV with width 5 meV (see Figure 8 d). The mass ratio of $^{13}C_6H_6$ and $^{12}C_6H_6$ is 84:78. The vibrational mode for the $^{13}C_6H_6$/Pt junction was predicted to shift from 42 meV ($^{12}C_6H_6$/Pt junction) to 40 meV assuming the harmonic oscillator model. The good agreement between the predicted and experimental values indicates that the benzene molecule bridged between Pt electrodes.

The number of benzene molecules bridging the Pt electrodes was evaluated by simultaneous conductance and shot noise measurements. The noise power is given by $S = 2eV\coth\left(\frac{eV}{2kT}\right)\frac{2e^2}{h}\sum\tau_i(1-\tau_i) + 4kT\frac{2e^2}{h}\sum\tau_i^2$, where τ_i is the transmission probability of the transmission channels across the junction.[16,17] The conductance is given by $G = \frac{2e^2}{h}\sum\tau_i$. Therefore, the number of transmission channels and their transmission probabilities could be determined by the simultaneous conductance and shot noise measurements. Figure 9 shows shot noise for the benzene/Pt junctions as a function of bias current. The transmission probabilities were ($\tau_1 = 0.68$, $\tau_2 = 0.40$), ($\tau_1 = 0.36$, $\tau_2 = 0.25$, $\tau_3 = 0.10$), and ($\tau_1 = 0.20$) for the benzene/Pt junctions with zero-bias conductances of 1.08, 0.71, and 0.20 G_0, respectively. The number of conduction channels roughly decreased with the decrease in conductance of the junction. The number of channels was one for the junction with a conductance of 0.2 G_0, which indicates that the number of molecules bridging Pt electrodes was one. IETS, shot noise, and conductance measurements confirmed the chemical species (benzene) and the number of molecules (one) bridging the Pt electrodes for the benzene/Pt junction with a conductance of 0.20 G_0. The single-molecule junction was well characterized using experimental methods.

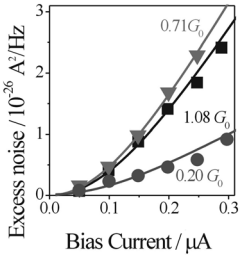

Figure 9. Shot noise as a function of the bias current across the Pt/benzene junction taken at a zero-bias conductance of 1.08 (■), 0.71 (▼), and 0.2 G_0 (●).[6]

The electron-transport properties and vibrational modes of the benzene molecule junction were further investigated by theoretical calculations (see Figure 10). The calculation results confirmed the experimental results. The conductance of the single benzene/Pt junction was 0.1–1 G_0, depending on the atomic configuration. During the junction stretching, the benzene molecule was initially positioned on the Pt electrodes with its plane perpendicular to the Pt junction axis. The conductance of the single benzene molecule junction with this configuration was about 1 G_0. Then, the benzene molecule was progressively tilted together with a continuous decrease in the conductance. The experimentally observed vibrational mode of

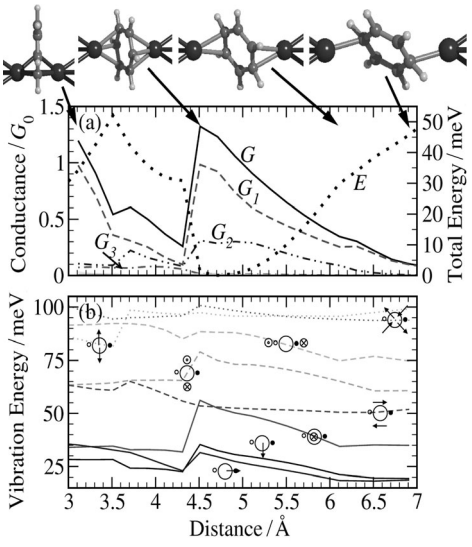

Figure 10. Simulation of the stretching process of a Pt/benzene junction. a) Total conductance *G*, the contribution of the individual conduction channels G_i, and the change in total energy *E* as a function of the distance between the Pt tip atoms. b) Stretching dependence of the energy of the benzene vibration modes in the range between 0 and 105 meV. The character of the modes is indicated by symbols, where benzene is represented by a large circle, the Pt atoms by two small circles, and arrows depict the motion of the molecule.[6]

42 meV is assigned to the hindered rotation mode of the benzene molecule bridging between the Pt electrodes.

4.2. Benzene/Au, Ag Junction

While the single benzene/Pt junction showed a high conductance value, it was not fixed. To obtain a single benzene molecule junction with a fixed conductance value, the benzene/Au and benzene/Ag junctions were investigated.

Figure 11 shows the conductance traces and histogram of the Ag contacts after the introduction of benzene.[38] The conductance traces show steps at integer multiples of 0.2 G_0

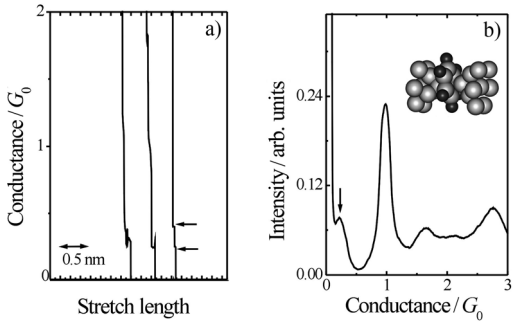

Figure 11. a) Typical conductance traces and b) histogram of the Ag contact after introduction of benzene molecules.[38]

(arrows in Figure 11 a), and the corresponding conductance histogram shows a peak at 0.2 G_0 (arrow in Figure 11 b). The single benzene molecule junction, which has a high and fixed conductance value, was fabricated using Ag electrodes. The existence of the benzene molecule between the Ag electrodes was confirmed by IETS. The IETS spectrum showed a peak around 40 meV, corresponding to the vibrational mode between benzene and Ag.[39] According to theoretical calculations, the adsorption energy of benzene on Ag(111) is smaller than that of benzene on Pt(111) by a factor of approximately 15,[40,41] which shows that the interaction between Pt and the benzene molecule is much greater than that between Ag and benzene molecules. The most energetically stable single benzene molecule junction was formed during stretching of the Ag contact in the presence of benzene. When the single benzene/Ag junction was stretched, the junction broke due to weak interaction between the benzene molecule and the Ag electrodes. In contrast, the benzene/Pt junction is able to take on various atomic configurations during stretching of the junction due to the strong metal–molecule interaction. The moderate metal–molecule interaction is favorable to obtain a single-molecule junction showing a fixed conductance value. The smaller metal–molecule interaction also leads to the decrease in the conductance of the single benzene molecule junction using Ag electrodes compared to the single benzene/Pt junction.

While single benzene molecule junctions were formed for Pt and Ag electrodes, such junctions were not formed for Au electrodes. Figure 12 shows the typical conductance traces and

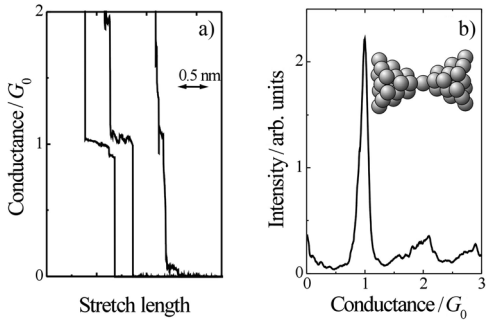

Figure 12. a) Typical conductance traces and b) histogram of the Au contact after introduction of benzene molecules.[38]

histogram of the Au contact after the introduction of benzene. The conductance trace shows a 1 G_0 plateau and the conductance histogram shows a clear 1 G_0 peak, which correspond to the clean Au contacts. The conductance trace rarely showed steps below 1 G_0, and no feature was observed below 1 G_0 in the conductance histogram, which indicated that the benzene molecule hardly bridged between Au electrodes. At low temperatures, an Au atomic chain is formed during the breaking of the Au contact.[42,43] After breaking the Au atomic chain, a nanogap is formed between the Au electrodes. The gap size was comparable to the length of the Au atomic chain. Therefore, the benzene molecule could not bridge between the Au electrodes due to the large size of the nanogap. In contrast, Ag did not form a monoatomic chain during the breaking of the Ag contact even at low temperatures.[44] The gap size was not very large after breaking the Ag contact, and thus the benzene molecule could bridge between the Ag electrodes.

4.3. C_{60} Molecule Junction

Single-molecule junctions with a high and fixed conductance value were also fabricated using C_{60}.[15,37,45] Figure 13 shows the conductance histogram of the Au, Ag, and Pt contacts after the introduction of C_{60} in UHV at 300 K. C_{60} was deposited on the metal contacts with a Knudsen cell before stretching and the conductance histograms show clear peaks indicating the formation of a single C_{60} molecule junction with fixed conductance values. The conductances of the C_{60}/Au, C_{60}/Ag, and C_{60}/Pt junctions were determined to be (0.3 ± 0.1), (0.5 ± 0.1), and (0.7 ± 0.1) G_0, respectively. The C_{60}/Pt junction showed a

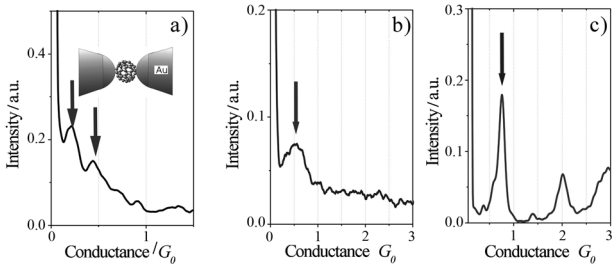

Figure 13. Conductance histograms of the a) Au, b) Ag, and c) Pt contacts after introduction of C_{60} molecules at 300 K.

fixed conductance value in contrast to the benzene/Pt junction. The difference was explained based on the shape of the molecule. The conductance of the benzene/Pt junction varied up to 10 times depending on the atomic configuration of the junction. In contrast to benzene, C_{60} is a spherical molecule. During the junction stretching, the out-of-plane molecular orientation did not change due to the spherical molecular shape of C_{60}, although the in-plane molecular orientation could change. Therefore, the C_{60} single-molecule junction showed a fixed conductance value due to the poor validity of the atomic configuration of the junction. The suitability of fullerene-based anchoring groups for the single-molecule junction was investigated using the MCBJ technique in solution.[46] Compared to thiols, the single-molecule junction with the fullerene-based anchoring groups gave a smaller spread in conductance than that with conventional anchoring groups.

The direct binding of π-conjugated molecules to metal electrodes leads to effective hybridization between the metal π orbitals. In the single π-conjugated molecular junction, electrons transport across the π orbital (HOMO or LUMO) and, therefore, the direct binding provides high conductivity of the single-molecule junction.

4.4. Other Related Systems

The direct binding of π-conjugated molecules to metal electrodes of tetrathiafulvalene (TTF) and tetraselenafulvalene (TSF) molecule junctions has been investigated.[47] These molecules were connected to Au electrodes in a face-to-face configuration. The conductances of the single TTF and TSF molecular junctions were 0.02 and 0.003 G_0, respectively, which is low in comparison to other C_{60} and benzene molecular junctions.

Relating to the direct binding of π-conjugated molecules to metal electrodes, direct Au–C binding was investigated using disubstituted alkane molecules terminated with trimethyltin ($SnMe_3$).[48] The C–$SnMe_3$ bond was cleaved and the Au–C bond was formed when the Au contacts were broken in the presence of a disubstituted alkane molecule terminated with $SnMe_3$. The conductance of the single alkane molecule junction having the direct Au–C bond was 100 times larger than that with a conventional anchoring group–metal bond (cf. Au–S, Au–NH_2).

5. π-Stacked Systems

In the previous section, we showed that the direct binding of π-conjugated molecules to metal electrodes is an efficient technique for the fabrication of highly conductive single-molecule junctions. As a next step, it is interesting to investigate single π-stacked systems where the top and bottom π-conjugated molecules directly bind to the metal electrodes, and electrons are transported through stacked π molecules. Electron transport through the noncovalently bound, π-stacked systems has been of particular interest and plays a vital role in biological systems, organic electronics, and polymer and materials science, typically on the macroscopic level and in bulk.[49,50] However, electron transport through π-stacked systems has never been directly examined because creating molecular junctions of stacked π molecules between electrodes is nontrivial.

Wu et al. tried to investigate electron transport through the π-stacked system using oligo(phenylene ethynylene) (OPE) molecules.[51] They investigated the conductance of OPE molecules with two anchoring groups, only one of which was a thiol. Significant electron transport was observed even for the OPE molecules with only one thiol anchoring group. Electrons were transported through the aromatic π–π coupling between adjacent molecules.

Recently, the efficient and precise assembly of stacked π systems was achieved using columnar coordination cages (see Figure 14).[52] Conductance measurements of these π-stacked systems were performed using the STM-BJ technique.[53] Figure 15a and b show the typical conductance trace and histogram of Au contacts in a solution containing inclusion complexes **1**·(**4**)$_2$. The trace shows a plateau in which the conductance is nearly constant (arrows in Figure 15a), and the conductance value of the plateau is an integer multiple of 6×10^{-4} G_0. The corresponding conductance histogram shows a peak at 6×10^{-4} G_0. When a solution of empty cage **1** was measured, no plateaus or peaks were observed in the conductance trace or histogram in the range $0.03–5\times10^{-5}$ G_0 and the measured conductance behavior was quite similar to that of the blank aqueous solution (see Figure 15c,d). Thus, inclusion complex **1**·(**4**)$_2$ was conductive, and electrons were transported through four π-stacked molecules (two molecules of guest **4** and two molecules of panel ligand **6**). From repeated measure-

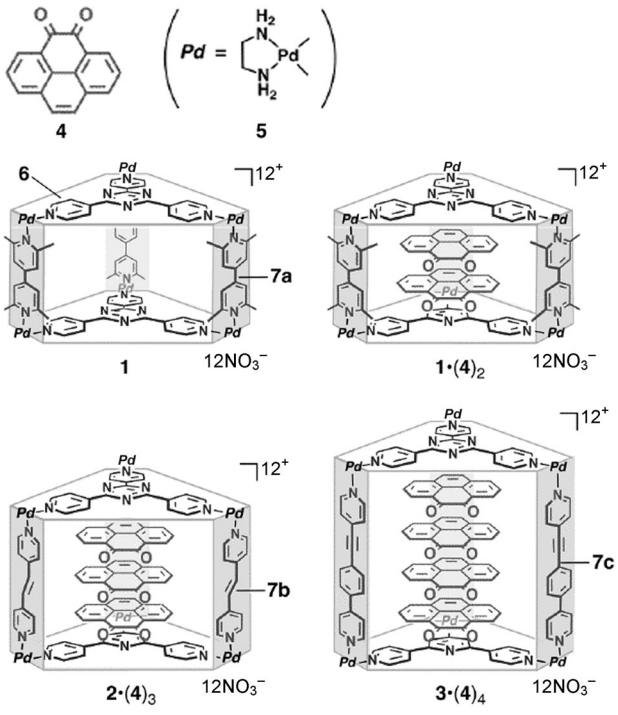

Figure 14. Structure of coordination cage **1** and π-stacked systems **1**·(**4**)$_2$, **2**·(**4**)$_3$, and **3**·(**4**)$_4$. The inclusion complexes **1**·(**4**)$_2$, **2**·(**4**)$_3$, and **3**·(**4**)$_4$, were prepared by simply mixing guest **4** with (en)Pd(ONO_2)$_2$ (**5**, en = ethylenediamine), panel ligand **6**, and pillar ligand **7a–c** in water.

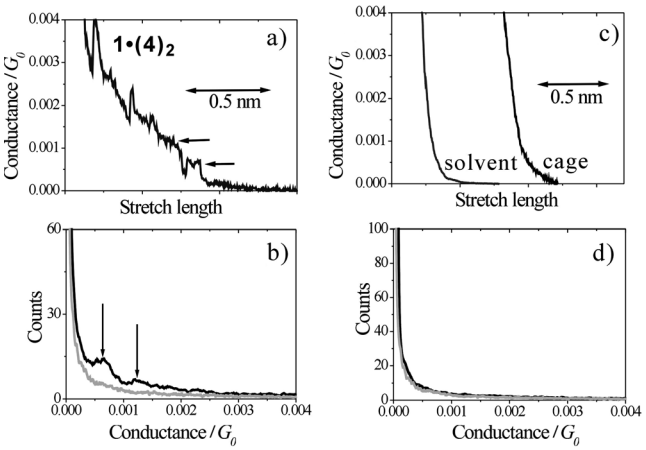

Figure 15. a,c) Conductance traces and b,d) histograms of Au contacts in water containing a,b) **1**·(**4**)$_2$ and c,d) empty cage **1**. The gray line indicates the result of the blank aqueous solution used as standard. The conductance histograms were constructed from 1000 conductance traces.[53]

ments, the conductance of the single π-stacked junctions of **1**·(**4**)$_2$, **2**·(**4**)$_3$, and **3**·(**4**)$_4$ were determined to be $(6\pm3)\times10^{-4}$, $(4\pm2)\times10^{-4}$, and $(2.5\pm0.6)\times10^{-4}$ G_0, respectively.

Figure 16 shows the distance dependence of conductance for the single π-stacked molecule junctions of **1**·(**4**)$_2$, **2**·(**4**)$_3$, and **3**·(**4**)$_4$, together with the typical single-molecule junctions. In

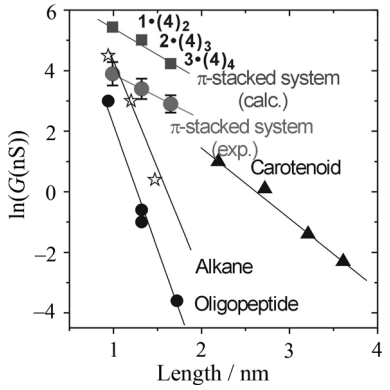

Figure 16. a) Distance dependence of observed conductance G for single π-stacked junctions **1**·(**4**)$_2$, **2**·(**4**)$_3$, and **3**·(**4**)$_4$. Typical single-molecule conductances for saturated (alkane chains and peptides) and conjugated (carotenoids) organic molecules are also shown.[53]

general, the conductance (G) of a short molecular junction is given by $G=A_N\exp(-BL)$, where A_N is a constant, L is the molecular length, and B is an exponential prefactor that depends on the electronic structure of the molecular junction.[54] Since the value of B roughly decreases with the decrease in the HOMO–LUMO gap, conductive molecules have small B values whereas insulating molecules have large ones. The B value for single-molecule π-stacked systems was 0.1 Å^{-1}, derived from the slope of L versus ln$G$ plots, and was smaller than that of insulating alkane chains ($B=0.7$–0.9 Å^{-1})[24,55] and comparable to that of conductive π-conjugated organic molecules ($B=0.05$–0.2 Å^{-1}).[56]

The atomic structure of the single π-stacked molecular junctions was investigated by statistical analysis of the conductance traces. Figure 17a shows a typical conductance trace of

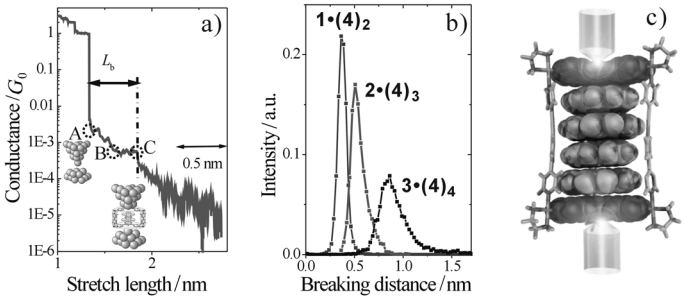

Figure 17. a) Conductance trace of the Au contact in solution containing **1**·(**4**)$_2$. b) Distribution of breaking distances (L_b) for **1**·(**4**)$_2$, **2**·(**4**)$_3$, and **3**·(**4**)$_4$. c) Schematic view of the single π-stacked molecule junction.[53]

the Au contact in a solution containing inclusion complex **1**·(**4**)$_2$. Just after breaking the Au atomic contact, a nanogap of finite size (≈0.4 nm) was formed due to the elastic response of banks of the electrodes.[57] The gap size increased when the contact was stretched and was roughly equal to the sum of the initial gap of ≈0.4 nm and the stretched length from this breaking point (A). Figure 17b shows the distribution of gap sizes (L_b) for inclusion complexes **1**·(**4**)$_2$, **2**·(**4**)$_3$, and **3**·(**4**)$_4$. The average size of the final gap increased by 0.24 nm per π-stacked molecule **4**. The value of 0.24 nm was close to the incremental increase in the molecular height of the π-stacked molecule per π-stacked molecule **4** (0.30 nm). The good agreement between these two values indicated that the top and bottom triangular aromatic panels of the π-stacked system were bound to the Au electrodes, as shown in Figure 17c.

The electron-transport properties of the single π-stacked molecule junction were investigated using theoretical calculations. Figure 18a shows the cluster model consisting of panel ligands **6**, π aromatic molecules (**4**)$_n$, and Au(111) 6×6 electrodes. To reduce the calculation time, organic pillars **7** and (en)Pd^{2+} units were removed and aromatic stacks (**6**)·(**4**)$_n$·(**6**) ($n=2$–4) were used as simple models for **1**·(**4**)$_2$, **2**·(**4**)$_3$, and **3**·(**4**)$_4$, respectively. The conductance of model π-stacks (**6**)·(**4**)$_n$·(**6**) ($n=2$–4) sandwiched between Au(111) electrodes was calculated from the transmission profile in Figure 18b and the conductance values were plotted in Figure 16. From the slope of the calculated conductance values, the value of B for the single (**6**)·(**4**)$_n$·(**6**) molecule junctions was estimated to be 0.13 Å^{-1}. This value was nearly identical to the obtained experimental B value and reinforces that, for inclusion complexes **1**·(**4**)$_2$, **2**·(**4**)$_3$, and **3**·(**4**)$_4$, electron transfer primarily occurred though the π-stacked systems. The calculations confirmed the efficient conductance of the π-stacked complexes. First, all (**6**)·(**4**)$_n$·(**6**) assemblies possess small HOMO–LUMO gaps (peaks C, D and A, B at −0.2 and +0.1 eV, respectively, in Figure 18b), which are important for efficient conduction. Second, the orbi-

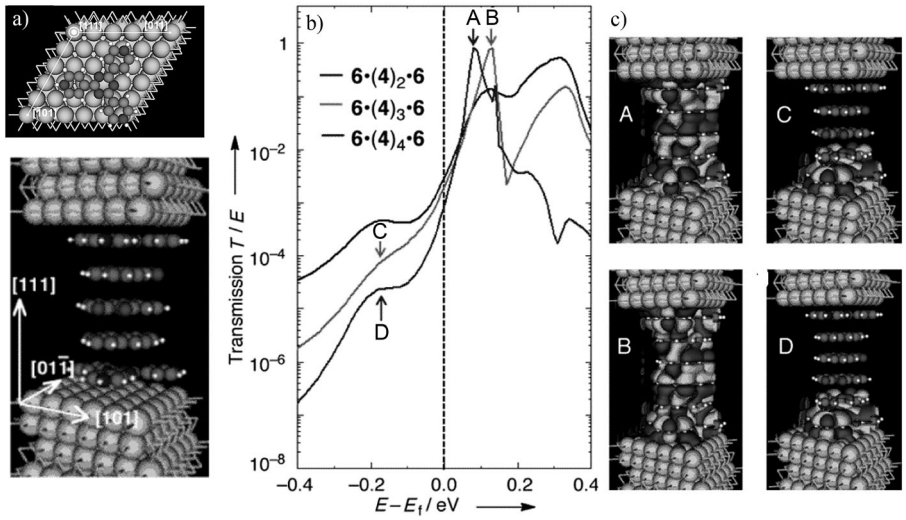

Figure 18. a) Top view of the π-stack model. The panel ligand **6** and the Au electrode connected to the ligand are depicted for the sake of simplicity. b) Calculated transmission curves for model π-stacks (**6**)·(**4**)$_n$·(**6**) ($n=2$–4). c) LUMO (A, B) and HOMO (C, D) projected onto the topmost layers of Au electrodes and the model π-stacks: A, C) (**6**)·(**4**)$_3$·(**6**) and B, D) (**6**)·(**4**)$_4$·(**6**).

tal overlap between the neighboring molecules (0.01 for LUMO–LUMO) is sufficient for orbital-delocalization and electron-transport pathways (see Figure 18c, A, B). Finally, the in-phase (bonding) relationship between the panel ligand **6** and the Au(111) electrode surface in the HOMOs (Figure 18c C, D) supports the strong Au–π interaction, which leads to the formation of stable single π-stacked molecular junctions.

Schneebeli et al. also succeeded in investigating electron transport through π-stacked systems.[58] The target molecule was the stacked benzene rings (up to four) held together in an eclipsed fashion via a paracyclophane scaffold. The dependence of the conductance on the number of benzene rings was investigated. The obtained B value of 0.63 Å^{-1} was smaller than the value observed for alkanes. The analysis of the conductance traces revealed that the electrodes were bound to the outermost benzene rings of the π–π-stacked molecular wires.

6. Summary and Outlook

In this review, we have discussed the fabrication, characterization, and control of the single-molecule junction. In particular, we have focused on the electron-transport properties of the single π-conjugated molecule junction, benzene, C_{60}, and π-stacked molecules.

The recent development of fabrication techniques such as STM-BJ and MCBJ enable us to investigate the electron-transport properties of a variety of molecules, including H_2, H_2O, DNA, and supermolecules. Electron transport through the π-stacked system was revealed thanks to recent developments in measurement techniques and chemical synthesis. While a variety of single-molecule junctions have been fabricated, the characterization of these junctions is still a challenging topic. In this review, we discussed the characterization of the single benzene molecule junction using IETS while making simultaneous conductance and shot noise measurements. While this benzene system was well characterized, most of the single-molecule junctions were not fully characterized by spectroscopic tools and further development of the IETS and shot noise measurements is required. The thermoelectricity in molecular junctions (Seebeck coefficient) provides information regarding the electronic structure of the single-molecule junction, and investigation of the thermoelectricity of the single-molecule junction is also a topic of great importance.

Control over the single-molecule junction will be a central topic in this research field in the coming years. At present, most works investigate the single-molecule junction using molecules that have important functions in bulk (e.g. photochromic molecules). However, it was found that the single-molecule junction did not always perform as expected from bulk studies. As we discussed before, the single-molecule junction using photochromic molecules did not switch from the off state to the on state while, on the other hand, it switched from the on state to off state via photoirradiation. It is promising to find novel functions which are characteristic of the single-molecule junction. Chemical reactions (catalytic reaction) can proceed on a metal surface, that is, at the metal/molecule interface. In the single-molecule junction, the molecule interacts with the metal surface via two interfaces. We can expect novel chemical reactions in the single-molecule junction, which cannot proceed in the gas phase and on metal surfaces.

Acknowledgements

We thank Prof. Jan van Ruitenbeek and Prof. Kei Murakoshi for their encouragement in the field of single atom and molecule junctions. We also thank our many collaborators, Prof. Makoto Fujita, Prof. Satoshi Watanabe, Dr. Tomofumi Tada, Dr. Takashi Murase, and the members of our laboratory.

Keywords: conjugated molecules · electron transport · interfaces · molecular electronics · single-molecule studies

[1] J. C. Cuevas, E. Scheer, *Molecular Electronics*, World Scientific, Singapore, **2010**.
[2] A. Aviram, M. A. Ratner, *Chem. Phys. Lett.* **1974**, *29*, 277–283.
[3] M. A. Reed, C. Zhou, C. J. Muller, T. P. Burgin, J. M. Tour, *Science* **1997**, *278*, 252–254.
[4] B. Xu, N. J. Tao, *Science* **2003**, *301*, 1221–1223.
[5] R. H. M. Smit, Y. Noat, C. Untiedt, N. D. Lang, M. C. van Hemert, J. M. van Ruitenbeek, *Nature* **2002**, *419*, 906–909.

[6] M. Kiguchi, O. Tal, S. Wohlthat, F. Pauly, M. Krieger, D. Djukic, J. C. Cuevas, J. M. van Ruitenbeek, *Phys. Rev. Lett.* **2008**, *101*, 046801.
[7] L. Lafferentz, F. Ample, H. Yu, S. Hecht, C. Joachim, L. Grill, *Science* **2009**, *323*, 1193-1197.
[8] G. Sedghi, V. M. García-Suárez, L. J. Esdaile, H. L. Anderson, C. J. Lambert, S. Martín, D. Bethell, S. J. Higgins, M. Elliott, N. Bennett, J. E. Macdonald, R. J. Nichols, *Nat. Nanotechnol.* **2011**, *6*, 517 – 523.
[9] M. Tsutsui, M. Taniguchi, K. Yokota, T. Kawai, *Nat. Nanotechnol.* **2010**, *5*, 286 – 290.
[10] T. Tada, K. Yoshizawa, *ChemPhysChem* **2002**, *3*, 1035 – 1037.
[11] D. Djukic, K. S. Thygesen, C. Untiedt, R. H. M. Smit, K. W. Jacobsen, J. M. van Ruitenbeek, *Phys. Rev. B* **2005**, *71*, 161402.
[12] M. Kiguchi, R. Stadler, I. S. Kristensen, D. Djukic, J. M. van Ruitenbeek, *Phys. Rev. Lett.* **2007**, *98*, 146802.
[13] N. Okabayashi, Y. Konda, T. Komeda, *Phys. Rev. Lett.* **2008**, *100*, 217801.
[14] W. Y. Wang, T. Lee, I. Kretzschmar, M. A. Reed, *Nano Lett.* **2004**, *4*, 643 – 646.
[15] T. Böhler, A. Edtbauer, E. Scheer, *Phys. Rev. B* **2007**, *76*, 125432.
[16] D. Djukic, J. M. van Ruitenbeek, *Nano Lett.* **2006**, *6*, 789 – 793.
[17] O. Tal, M. Krieger, B. Leerink, J. M. van Ruitenbeek, *Phys. Rev. Lett.* **2008**, *100*, 196804.
[18] P. Reddy, S.-Y. Jang, R. A. Segalman, A. Majumdar, *Science* **2007**, *315*, 1568 – 1571.
[19] I. Díez-Pérez, J. Hihath, Y. Lee, L. Yu, L. Adamska, M. A. Kozhushner, I. I. Oleynik, N. Tao, *Nat. Chem.* **2009**, *1*, 635 – 641.
[20] D. Dulic, S. J. van der Molen, T. Kudernac, H. T. Jonkman, J. J. D. de Jong, T. N. Bowden, J. van Esch, B. L. Feringa, B. J. van Wees, *Phys. Rev. Lett.* **2003**, *91*, 207402.
[21] H. Song, Y. Kim, Y. H. Jang, H. Jeong, M. A. Reed, T. Lee, *Nature* **2009**, *462*, 1039 – 1043.
[22] N. Agraït, A. L. Yeyati, J. M. van Ruitenbeek, *Phys. Rep.* **2003**, *377*, 81 – 279.
[23] D. Dulic', F. Pump, S. Campidelli, P. Lavie, G. Cuniberti, and A. Filoramo, *Angew. Chem.* **2009**, *121*, 8423 – 8426; *Angew. Chem. Int. Ed.* **2009**, *48*, 8273 – 8276.
[24] F. Chen, X. Li, J. Hihath, Z. Huang, N. Tao, *J. Am. Chem. Soc.* **2006**, *128*, 15874 – 15881.
[25] M. Kiguchi, S. Miura, K. Hara, M. Sawamura, K. Murakoshi, *Appl. Phys. Lett.* **2006**, *89*, 213104.
[26] M. Kiguchi, S. Murata, K. Hara, M. Sawamura, K. Murakoshi, *Appl. Phys. Lett.* **2007**, *91*, 053110.
[27] Y. Ie, T. Hirose, H. Nakamura, M. Kiguchi, N. Takagi, M. Kawai, Y. Aso, *J. Am. Chem. Soc.* **2011**, *133*, 3014 – 3022.
[28] S. Grunder, R. Huber, S. Wu, C. Schonenberger, M. Calame, M. Mayor, *Eur. J. Org. Chem.* **2010**, 833 – 845.
[29] C. Li, I. Pobelov, T. Wandlowski, A. Bagrets, A. Arnold, F. Evers, *J. Am. Chem. Soc.* **2008**, *130*, 318 – 326.
[30] S.-H. Ke, H. U. Baranger, W. Yang, *J. Am. Chem. Soc.* **2004**, *126*, 15897 – 15904.
[31] K.-H. Müller, *Phys. Rev. B* **2006**, *73*, 045403.
[32] L. Venkataraman, J. E. Klare, I. W. Tam, C. Nuckolls, M. S. Hybertsen, M. L. Steigerwald, *Nano Lett.* **2006**, *6*, 458 – 462.
[33] L. Venkataraman, J. E. Klare, C. Nuckolls, M. S. Hybertsen, M. L. Steigerwald, *Nature* **2006**, *442*, 904 – 907.
[34] L. Venkataraman, Y. S. Park, A. C. Whalley, C. Nuckolls, M. S. Hybertsen, M. L. Steigerwald, *Nano Lett.* **2007**, *7*, 502 – 506.
[35] Z. Li, D. S. Kosov, *Phys. Rev. B* **2007**, *76*, 035415.
[36] Y. S. Park, A. C. Whalley, M. Kamenetska, M. L. Steigerwald, M. S. Hybertsen, C. Nuckolls, L. Venkataraman, *J. Am. Chem. Soc.* **2007**, *129*, 15768 – 15769.
[37] M. Kiguchi, *Appl. Phys. Lett.* **2009**, *95*, 073301.
[38] S. Kaneko, T. Nakazumi, M. Kiguchi, *J. Phys. Chem. Lett.* **2010**, *1*, 3520 – 3523.
[39] J. I. Pascual, J. J. Jackiw, Z. Song, P. S. Weiss, H. Conrad, H.-P. Rust, *Phys. Rev. Lett.* **2001**, *86*, 1050 – 1053.
[40] A. Bilić, J. R. Reimers, N. S. Hush, R. C. Hoft, M. J. Ford, *J. Chem. Theory Comput.* **2006**, *2*, 1093 – 1105.
[41] M. Saeys, M.-F. Reyniers, G. B. Martin, M. Neurock, *J. Phys. Chem. B* **2002**, *106*, 7489 – 7498.
[42] A. I. Yanson, G. R. Bollinger, H. E. van den Brom, N. Agrait, J. M. van Ruitenbeek, *Nature* **1998**, *395*, 783.
[43] R. H. M. Smit, C. Untiedt, A. I. Yanson, J. M. van Ruitenbeek, *Phys. Rev. Lett.* **2001**, *87*, 266102.
[44] W. H. A. Thijssen, D. Marjenburgh, R. H. Bremmer, J. M. van Ruitenbeek, *Phys. Rev. Lett.* **2006**, *96*, 026806.
[45] M. Kiguchi, K. Murakoshi, *J. Phys. Chem. C* **2008**, *112*, 8140 – 8143.
[46] C. A. Martin, D. Ding, J. K. Sørensen, T. Bjørnholm, J. M. van Ruitenbeek, H. S. J. van der Zant, *J. Am. Chem. Soc.* **2008**, *130*, 13198 – 13199.
[47] M. Taniguchi, M. Tsutsui, K. Shoji, H. Fujiwara, T. Kawai, *J. Am. Chem. Soc.* **2009**, *131*, 14146 – 14147.
[48] Z.-L. Cheng, R. Skouta, H. Vazquez, J. R. Widawsky, S. Schneebeli, W. Chen, M. S. Hybertsen, R. Breslow, L. Venkataraman, *Nat. Nanotechnol.* **2011**, *6*, 353 – 357.
[49] S. Bhosale, A. L. Sisson, P. Talukdar, A. Fürstenberg, N. Banerji, E. Vauthey, G. Bollot, J. Mareda, C. Röger, F. Würthner, N. Sakai, S. Matile, *Science* **2006**, *313*, 84 – 86.
[50] W. A. Schoonveld, J. Wildeman, D. Fichou, P. A. Bobbert, B. J. van Wees, T. M. Klapwijk, *Nature* **2000**, *404*, 977 – 980.
[51] S. Wu, M. T. González, R. Humber, S. Grunder, M. Mayor, C. Schönenberger, M. Calame, *Nat. Nanotechnol.* **2008**, *3*, 569 – 574.
[52] Y. Yamauchi, M. Yoshizawa, M. Akita, M. Fujita, *J. Am. Chem. Soc.* **2010**, *132*, 960 – 966.
[53] M. Kiguchi, T. Takahashi, Y. Takahashi, Y. Yamauchi, T. Murase, M. Fujita, T. Tada, S. Watanabe, *Angew. Chem.* **2011**, *123*, 5826 – 5829; *Angew. Chem. Int. Ed.* **2011**, *50*, 5708 – 5711.
[54] N. J. Tao, *Nat. Nanotechnol.* **2006**, *1*, 173 – 181.
[55] X. Xiao, B. Xu, N. J. Tao, *J. Am. Chem. Soc.* **2004**, *126*, 5370 – 5371.
[56] J. He, F. Chen, J. Li, O. F. Sankey, Y. Terazono, C. Herrero, D. Gust, T. A. Moore, A. L. Moore, S. M. Lindsay, *J. Am. Chem. Soc.* **2005**, *127*, 1384 – 1385.
[57] J. Zhao, K. Murakoshi, X. Yin, M. Kiguchi, Y. Guo, N. Wang, S. Liang, H. Liu, *J. Phys. Chem. C* **2008**, *112*, 20088 – 20094.
[58] S. T. Schneebeli, M. Kamenetska, Z. Cheng, R. Skouta, R. A. Friesner, L. Venkataraman, R. Breslow, *J. Am. Chem. Soc.* **2011**, *133*, 2136 – 2139.

Received: October 1, 2011
Published online on February 6, 2012

